ORIGINAL ARTICLE

Structural epicardial disease and microvascular function are determinants of an abnormal longitudinal myocardial blood flow difference in cardiovascular risk individuals as determined with PET/CT

Ines Valenta, MD,[a] Alessandra Quercioli, MD,[a] Gabriella Vincenti, MD,[a] René Nkoulou, MD,[a] Stephan Dewarrat, MSc,[b] Olivier Rager, MD,[b] Habib Zaidi, PhD,[b] Yann Seimbille, PhD,[b] Francois Mach, MD,[a] Osman Ratib, MD,[b] and Thomas H. Schindler, MD, PhD[a]

Background. The aim of this study was to determine whether epicardial structural disease may affect the manifestation of a longitudinal decrease in myocardial blood flow (MBF) or MBF difference during hyperemia in cardiovascular risk individuals, and its dependency on the flow increase.

Methods and Results. In 54 cardiovascular risk individuals (at risk) and in 26 healthy controls, MBF was measured with ^{13}N-ammonia and PET/CT in mL/g/min at rest and during dipyridamole stimulation. Computed tomography coronary angiography (CTA) was performed using a 64-slice CT of a PET/CT system. Absolute MBFs during dipyridamole stimulation were mildly lower in the mid-distal than in the mid-LV myocardium in controls (2.20 ± .51 vs 2.29 ± .51, $P < .0001$), while it was more pronounced in at risk with normal and abnormal CTA (1.56 ± .42 vs 1.91 ± .46 and 1.18 ± .34 vs 1.51 ± .40 mL/g/min, respectively, $P < .0001$), resulting in a longitudinal MBF difference that was highest in at risk with normal CTA, intermediate in at risk abnormal CTA, and lowest in controls (.35 ± .16 and .22 ± .09 vs .09 ± .04 mL/g/min, respectively, $P < .0001$). On multivariate analysis, log-CCS and mid-LV hyperemic MBF increase, indicative of microvascular function, were independent predictors of the observed longitudinal MBF difference ($P ≤ .004$ by ANOVA).

Conclusions. Epicardial structural disease and microvascular function are important determinants of an abnormal longitudinal MBF difference as determined with PET/CT. (J Nucl Cardiol 2010;17:1023–33.)

Key Words: Coronary artery disease · coronary circulation · endothelial function · myocardial blood flow · positron emission tomography

INTRODUCTION

Measurements of myocardial blood flow (MBF) with PET at rest and its responses to sympathetic stimulation with cold pressor testing or pharmacologically stimulated coronary flow increases afford the non-invasive identification and characterization of coronary circulatory function in normal and diseased vascular states.[1-4] Hyperemic MBFs are considered to denote predominantly endothelium-independent flow responses owing to the relaxation of the vascular smooth muscle cells of the arteriolar vessels during pharmacologic vasodilation.[1,2] Shear sensitive components of the

coronary endothelium, however, contribute through flow-mediated coronary vasodilation to the overall hyperemic flow during pharmacologic vasodilation.[1,2] As hyperemic MBFs during pharmacologic vasodilation comprise up to 21-25% flow-mediated and, thus, endothelium-related vasodilatory effects, it is also reported as the ''total integrated coronary circulatory function.''[1,2,5,6] Conversely, functional and/or structural abnormalities of the coronary arterial wall may impair flow-mediated coronary vasodilation predominantly of the epicardial artery.[7-10] Such functional alterations or diffuse epicardial narrowing of the epicardial arteries,[7,9,11] commonly accompanied by an impairment of flow-mediated vasodilation, have been suggested as cause for a more recently described longitudinal decrease in myocardial perfusion or MBF during pharmacologically stimulated hyperemia.[7-9] Until recently, PET flow studies assessing the longitudinal base-to-apex MBF gradient during pharmacologic vasodilation did not provide information on the presence of structural coronary artery disease (CAD). Thus, it remains uncertain how the presence or absence of structural alterations of the epicardial artery may affect the manifestation of an abnormal longitudinal, base-to-apex MBF gradient during higher coronary flows. Another aspect is that, according to the Hagen–Poiseuille equation, the velocity of coronary flow represents a major determinant of the intracoronary resistance, apart from the fourth power of the vessel diameter. According to this, a longitudinal, base-to-apex MBF gradient during hyperemic flows, most likely reflecting an impairment of a flow-mediated coronary vasodilation and/or structural CAD, should be more pronounced with higher flow increases as a consequence of higher increases in intracoronary resistance associated with a pressure drop along the epicardial artery.[12]

With this in mind, we aimed to investigate whether epicardial structural disease, as evidenced by CTA-determined coronary morphology, may affect the manifestation of a longitudinal decrease in MBF from the mid to mid-distal segment of the left ventricle (LV) or longitudinal MBF difference during hyperemic flows in cardiovascular risk individuals, and its dependency on the hyperemic flow increase.

MATERIALS AND METHODS

Study Population

The study population comprised 54 cardiovascular risk individuals, who were referred for myocardial perfusion imaging with ^{13}N-ammonia and PET/CT (64-slice Biograph HiRez TruePoint PET-CT scanner, Siemens Medical Solutions,

Erlangen, Germany) for the evaluation of flow-limiting CAD (Table 1). In addition, 26 healthy controls without known cardiovascular risk factors undergoing the same imaging protocol served as controls. In these individuals, coronary calcium score (CCS) was determined and non-invasive computed tomography coronary angiography (CTA) was performed with 64-slice CT of the PET/CT system. Only individuals with normal stress–rest perfusion imaging, evaluated semiquantitatively on ^{13}N-ammonia PET/CT, were included for study purpose. The study population was grouped as follows: group 1, healthy controls with normal CTA; group 2, cardiovascular risk individuals with normal CTA; and group 3, cardiovascular risk individuals but with evidence of both calcified and non-calcified coronary plaque burden on CTA (abnormal CTA). Individuals who presented only minor non-calcified plaque burden were not included for study analysis. Cardiovascular risk factors included the presence of arterial hypertension, smoking, type 2 diabetes mellitus, hypercholesterolemia, or family history of CAD. Patients with evidence of left ventricular hypertrophy on the electrocardiogram were excluded from study analysis. Vasoactive medications such as calcium channel blockers, angiotensin-converting enzyme inhibitors, statin as well as β-blockers, and diuretics were discontinued at least 24 hours before PET flow study during pharmacologic vasodilation with dipyridamole and at rest. All study participants refrained from caffeine-containing beverages for $\geq$24 hours and from smoking for $\geq$12 hours prior to the PET study. The study was approved by the University Hospitals of Geneva Institutional Review Board (No. 07-184), and each participant signed the approved informed consent form.

Calcium Scanning

Prior to PET flow studies, 64-slice multidetector computed tomography (MDCT) of the Biograph HiRez TruePoint PET-CT scanner (Siemens) determined coronary artery calcium score (CCS). The scanner was operated in the single slice mode with an image acquisition time of 100 ms and a section thickness of 3 mm. Prospective ECG-triggering was done at 55% of the R–R interval. Contiguous slices to the apex of the heart were obtained. CCS was considered present if three or more contiguous pixels with a signal intensity of >130 HU were identified.[13] The size of the lesion was automatically calculated, and the CCS was scored using the Agatston algorithm.[13] The CCS was computed across all lesions denoted within the left main, left anterior descending artery (LAD), left circumflex artery (LCx), and right coronary artery (RCA), and the sum of all lesion scores yielded the total CCS.

PET Flow Studies

Following the topogram used to determine the axial field of view and a low-dose CT scan (120 kV, 30 mA) for attenuation correction, PET emission data were acquired during shallow breathing. PET imaging during dipyridamole-stimulated hyperemia (140 μg/kg/min) and at rest was commenced immediately following injection of approximately

Table 1. Clinical characteristics of the study population

	Controls	At risk with normal CTA	At risk with abnormal CTA
Numbers (N)	26	26	28
Age (years)	38 ± 10	55 ± 12*	72 ± 10*[†]
BMI (kg/m^2)	23 ± 3	33 ± 11*	26 ± 5*[†]
CCS (HU)	0	0	962 ± 933
Risk factors			
Hypertension (N)	0	7 (27%)	7 (25%)
Smoking (N)	0	10 (38%)	13 (46%)
Hypercholesterolemia (N)	0	10 (38%)	17 (61%)
Obesity (N)	0	11 (42%)	4 (14%)
Family history of CAD (N)	0	7 (27%)	5 (18%)
Diabetes mellitus (N)	0	5 (19%)	8 (29%)
Fasting plasma concentrations			
Cholesterol (mg/dL)	203 ± 33	208 ± 41	214 ± 45
LDL (mg/dL)	128 ± 38	136 ± 35	147 ± 30*
HDL (mg/dL)	54 ± 21	44 ± 12*	43 ± 11*
TG (mg/dL)	107 ± 78	130 ± 63	122 ± 39
Glucose (mg/dL)	92 ± 12	102 ± 13*	110 ± 21*
CRP (mg/dL)	1.8 ± 1.9	5.9 ± 9.2*	12.2 ± 15.8*

Numbers, N (%).
BMI, Body mass index; *CCS*, coronary artery calcium score; *LDL*, low-density lipoprotein; *HDL*, high-density lipoprotein; *TG*, triglyceride; *CRP*, C-reactive protein.
*$P \leq .05$ vs controls and [†]$P \leq .05$ vs at risk without CAC (*t*-test for independent samples).

500-600 MBq of ^{13}N-ammonia for a total duration of 18-min list-mode PET data acquisition, respectively. The stress and rest PET images were visually checked for accurate alignment with the CT scan used for attenuation correction. In case of misalignment between PET and CT images, CT data were shifted in the horizontal and vertical directions in the transaxial planes and in the superior-inferior direction of coronal planes to visually align the heart borders visible on CT with the PET emission data to achieve an accurate coregistration.[14] The reoriented ^{13}N-ammonia images and the corresponding polar maps were generated from the last 720-s image set and they were also evaluated visually and semiquantitatively for stress and rest regional perfusion abnormalities. The PET images were assessed with a 17-segment model and a 5-point grading system by two expert observers.[15] Summed stress score (SSS), summed rest score, and summed difference score (SDS) were calculated.[16] An SSS <4 was considered normal, 4-8 mildly abnormal, 9-13 moderately abnormal, and >13 severely abnormal perfusion. Further, an SDS ≥ 2 identified ischemia, whereas <2 was considered a normal. Image interpretation was visually performed in consensus by two nuclear cardiologists. In the case of disagreement between observers, consent was achieved in a joint reading.

Beginning with intravenous ^{13}N-ammonia application, serial transaxial emission images were recorded (12 images per frame of 10 s each, 3 frames of 20 s each, and 6 frames of 30 s each) with PET/CT, and time-activity curves from the first 12 dynamic frames (12 for 10 s each) in conjunction with a two-compartment tracer kinetic model[17] were used to calculate regional and global MBF in mL/g/min. On the polar map of the last 720-s image set, regions of interest (ROIs) were assigned to the territories of the three coronary arteries using the 17-segment model.[18] Applying the PMOD software package (version 2.8 PMOD Technologies Ltd., Zurich, Switzerland), MBF was determined in mL/g/min.[19] The tracer kinetic model applied, corrected for physical decay of ^{13}N-ammonia, partial-volume-related underestimations of true myocardial tissue concentrations (by assuming a uniform myocardial wall thickness of 1 cm),[20,21] and spillover of radioactivity between the left ventricular blood pool and myocardium.[22] Regional MBFs of the LAD, LCx, and RCA territory were averaged on a polar map and the resulting mean MBF of the LV was defined as global MBF. In addition, the assessment of longitudinal flows, MBFs in the mid and mid-distal myocardial segment of the LV corresponding to the vascular territories of the LAD (segments: 7-8 and 13-14), LCx (segments: 11-12 and 16), and RCA (segments: 9-10 and 15) were determined. Basal segments (LAD: 1-2, LCx: 5-6, and RCA: 3-4) and the apical segment (LAD: 17), however, were not included for this analysis owing to a possible count variability induced by the membranous septum, by a certain variability in locating the last apical slice, and by partial volume errors resulting from object size at the apex.[7] A decrease in MBF from mid to mid-distal LV myocardium was defined as longitudinal MBF

difference (mL/g/min) indicative of a perfusion gradient. Changes in the longitudinal MBF difference from rest to dipyridamol-stimulated hyperemia were defined as rest-to-stress change in longitudinal MBF difference (Δ longitudinal MBF difference = longitudinal MBF difference during hyperemia minus longitudinal MBF difference at rest). Heart rate, blood pressure, and a 12-lead electrocardiogram were recorded continuously during each MBF measurement. From the average of heart rate and systolic blood pressure during the first 2 min of each image acquisition, the rate-pressure product (RPP) was derived as an index of cardiac work. To account for possible interindividual variations in coronary driving pressure, an index of global coronary vascular resistance (CVR) was determined as the ratio of mean arterial blood pressure (mmHg) to MBF (mL/g/min).

64-Slice MDCT Scanning Protocol

Following PET perfusion imaging, low-dose CTA using the ECG-dependent dose modulation (''ECG-pulsing'') on a dedicated 64-slice Biograph HiRez TruePoint PET-CT scanner (Siemens) was performed in order to delineate coronary morphology. Metoprolol was applied intravenously (5-40 mg) (Lopressor, AstraZeneca) prior to CTA examination to achieve the target heart rate of <65 bpm. Coaching and training of the patient (practice of breath-hold) was performed before CT scanning to avoid breathing artifacts. In addition, all patients received isosorbide dinitrate 2.5 mg sublingual (Isoket spray, Schwarz Pharma) to ascertain a maximal vasodilation of epicardial artery. For CTA, 80 mL of iomeprol (Iomeron 400, Bracco-Altana Pharma) was infused at a flow rate of 5 mL/s followed by 50 mL saline solution into an antecubital vein via an 18-gauge catheter. Bolus tracking was performed after the injection of 20 mL of contrast agent (5 mL/s) by positioning an ROI into the ascending aorta. CTA was performed with retrospective gating, using the available tube current modulation tool referred to as ''ECG-pulsing.'' Scanning parameters were $64 \times .6$ mm^2 collimation, gantry rotation time 330 ms, a pitch of .2, and pulse window 70% of the R–R cycle. Tube voltage and tube current were adapted to the body mass index (BMI) as described previously.[23]

CTA Image Interpretation

CTA images were analyzed visually and independently by two experienced observers on axial source images, multiplanar and curved reformations, and thin-slab maximum intensity projections using the 2D/3D visualization software Vitrea 2 (Vital images, Inc.). Image quality for each data set was evaluated on a five-scale score. Coronary arteries were analyzed according to a 15-segment model proposed by the American Heart Association.[24] Each segment was visually analyzed on at least two planes, one parallel and one perpendicular to the course of the vessel with regard to coronary artery delineation, and all vessels with a diameter down to 1.5 mm were included in the analysis. The coronary artery diameter in a non-branching vessel segment of the proximal LAD, LCx, and RCA was evaluated in both longitudinal and short axis views.[24] The reported diameters of the proximal coronary segments for each study participant resulted from the average of both measurements. For each segment, both presence of atherosclerotic plaque and its composition were determined. Atherosclerotic lesions were identified as morphologically significant if the diameter stenosis was ≥50%. Plaque lesions below this threshold were classified as mild and non-significant lesions. Plaque composition was graded as non-calcified plaque (plaques having lower density than contrast enhanced lumen), calcified plaque (plaques with high density), and mixed plaques (composition of both non-calcified and calcified plaque burden).[25]

Statistics

Data are presented as the mean ± SD for quantitative and absolute frequencies for qualitative variables. For comparison of differences, appropriate t-tests for independent or paired samples were used. Pearson's correlation coefficient (r), assuming a linear regression, was calculated to investigate possible associations between MBF and CVR, hemodynamic and cardiovascular risk parameters. Since CCSs followed a skewed distribution, the CCSs were logarithmically transformed (log-CCS) and related to the MBF and CVR data. In addition, cardiovascular risk individuals with abnormal CTA and CAC were also grouped according to tertiles of log-CCS with <69.3 HU (lowest tertile), between 69.3 and 361.5 HU (medium tertile), and >361.5 HU (highest tertile). Multivariate analysis was performed with the logistic regression model. Coronary non-calcified plaque burden and proximal artery diameter were not entered into the multivariate model, because they correlated with log-CCS.[26] Statistical significance was assumed if a null hypothesis could be rejected at $P = .05$. All statistical analyses were performed with SPSS for Windows 17.0 (SPSS).

RESULTS

Clinical Characteristics

Table 1 summarizes the clinical characteristics of the study population. In the cardiovascular risk group with normal CTA, 9 patients had one coronary risk factor, 12 patients had two, and 5 patients had three or more coronary risk factors. As regards the cardiovascular risk group with abnormal CTA, 7 patients had one coronary risk factor, 16 patients had two, and 5 patients had three coronary risk factors. In these cardiovascular risk individuals, 20 patients had CAC in three-, 6 in two-, and 2 in one coronary vessel with a mean CCS of 962 ± 933 HU (range 3.3-2678). A CCS <100, ≥100, and >400 was present in 6 (21%), 5 (18%), and 6 (21%), respectively. Eleven (39%) of these had a CCS >1000. Due to the high coronary calcification burden, however, 87 out of 420 (21%) coronary segments were not assessable for analysis of epicardial morphology. As far

as coronary artery segments could be evaluated, morphologically significant epicardial lesions (≥50% stenosis) could be identified in 7 (25%), whereas non-calcified plaque burden was observed in 9 (33%), and mixed plaques 25 (90%). Notably, in those seven cardiovascular risk individuals where epicardial lesions with ≥50% stenosis could be denoted by CTA, stress–rest ^{13}N-ammonia PET perfusion images were normal. As regards the mean coronary artery diameter of the proximal vessel segments of the LAD, LCx, and RCA on CTA, it did not differ significantly between controls and cardiovascular risk individuals with normal CTA (3.90 ± .50 vs 3.83 ± .49 mm, $P = .58$), whereas it was significantly higher in controls than in cardiovascular risk individuals with abnormal CTA (3.90 ± .50 vs 3.60 ± .50 mm, $P < .03$). Further, the mean proximal artery diameter tended to be higher in cardiovascular risk group with normal CTA than in the group with abnormal CTA (3.83 ± .49 vs 3.60 ± .50 mm, $P = .10$). The group comparison of the mean proximal artery diameter in controls with normal CTA was not significantly different from at risk groups with abnormal CTA ($P = .10$ by ANOVA). Finally, in the cardiovascular risk group with abnormal CTA, there was some correlation between the mean proximal artery diameter and log-CCS ($r = -.33$, SEE = .47; $P < .01$).

Global MBF Measurements and Hemodynamics

At rest, heart rate and systolic blood pressure and corresponding RPP were higher in at risk groups than in controls, whereas they were the highest in at risk with abnormal CTA (Table 2). The latter was paralleled by a progressive increase in resting MBF from controls to at risk groups with normal and abnormal CTA. During dipyridamole-stimulated hyperemia, heart rates had increased significantly from rest but they were comparable between groups (Table 2), whereas systolic blood pressure had non-significantly decreased from rest. There were no significant differences in heart rate or RPP during pharmacologic vasodilation among the three study groups, whereas global hyperemic MBFs were significantly higher in controls than in at risk groups (Table 2). Further, global hyperemic MBF was significantly lower in at risk group with abnormal CTA than in those with normal CTA. When the global hyperemic MBFs were related to the mean arterial blood pressure in order to account for possible interindividual variations in coronary driving pressure, the resulting estimates of global CVR (mean arterial blood pressure/MBF) mirrored the MBF values at rest and during pharmacologic vasodilation for each group studied. Thus, differences in coronary

Table 2. Myocardial flow parameters and hemodynamics during positron emission tomography

	Controls	At risk with normal CTA	At risk with abnormal CTA
Flow parameters			
Global MBF-rest	.71 ± .13	.89 ± .21*	.99 ± .22*
Global MBF-DP	2.29 ± .51	1.83 ± .49*	1.42 ± .38*[†]
Global MFR	3.28 ± .70	2.14 ± .73*	1.45 ± .30*[†]
Global CVR-rest	121 ± 23	104 ± 27*	91 ± 22*
Global CVR-DP	37 ± 9	50 ± 13*	60 ± 16*[†]
Global ΔCVR	−84 ± 20	−54 ± 27*	−32 ± 17*[†]
LMBF difference-rest	.05 ± .03	.09 ± .09*	.09 ± .06*
LMBF difference-DP	.09 ± .04	.35 ± .16*	.22 ± .09*[†]
ΔLMBF difference	.05 ± .05	.26 ± .14*	.14 ± .10*[†]
Hemodynamics			
Rest-HR (bpm)	63 ± 6	67 ± 12	70 ± 11*
DP-HR (bpm)	87 ± 10	83 ± 12	79 ± 12*
Rest-SBP (mmHg)	115 ± 11	124 ± 22	125 ± 18*
DP-SBP (mmHg)	113 ± 10	122 ± 22	119 ± 18*
Rest-RPP	7233 ± 756	8259 ± 1892*	8839 ± 2140*
DP-RPP	9896 ± 1451	10067 ± 2051	9494 ± 2282
ΔRPP	2663 ± 1317	1807 ± 1784	656 ± 919*

MBF, Myocardial blood flow (mL/g/min); *MFR*, myocardial flow reserve; *CVR*, coronary vascular resistance (mmHg/mL/g/min); *LMBF*, longitudinal MBF (mL/g/min); *HR*, heart rate; *SBP*, systolic blood pressure; *RPP*, rate-pressure product (HR × SBP).
*$P \leq .05$ vs controls and [†]$P \leq .05$ vs at risk without CAC (*t*-test, independent samples).

driving pressure during pharmacologic vasodilation can be widely ruled out as cause for alterations in hyperemic MBF responses. The group comparison of global hyperemic MBF and its corresponding CVR in controls was significantly different from at risk groups ($P < .0001$ by ANOVA).

In at risk group with abnormal CTA and CAC, we also evaluated a possible association between CAC burden and global MBFs. In this regard, the log-CCS was not related to global MBF at rest ($r = .02$, SEE = .81; $P = .91$), whereas significant and inverse associations between log-CCS and global hyperemic flows ($r = -.41$, SEE = .74; $P \leq .03$) and MFR ($r = -.51$, SEE = .70; $P \leq .006$) were noted. These observations were further substantiated, when global CVR was related to log-CCS. Also here, global CVR at rest was not correlated to log-CCS ($r = .07$, SEE = .81; $P = .72$). In contrast, global CVR during hyperemia and also the ratio of global CVR during hyperemia to CVR at rest significantly correlated with log-CCS, respectively ($r = .47$, SEE = .72; $P \leq .012$; and $r = .51$, SEE = .69; $P \leq .006$).
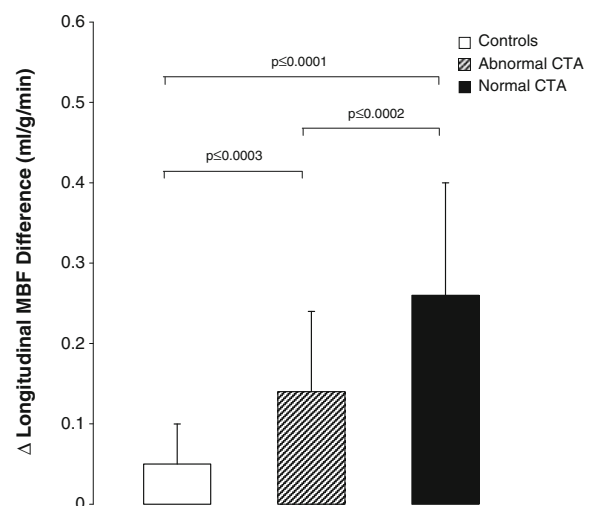
Longitudinal MBF Differences

Resting MBFs were significantly lower in the mid-distal than in the mid-LV myocardium in controls and in at risk groups with normal CTA and with abnormal CTA (.64 ± .13 vs .69 ± .13, .80 ± .22 vs 89 ± .24, and .91 ± .20 vs 1.00 ± .23 mL/g/min, respectively, $P < .0001$), resulting in longitudinal MBF differences of which were significantly higher in at risk groups than in controls
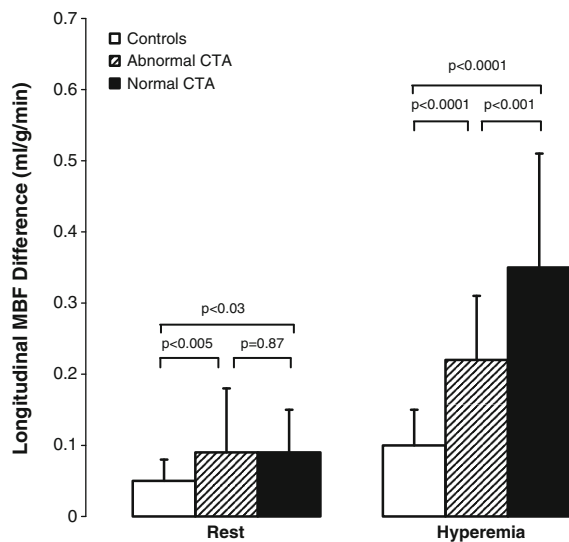
(Table 2) (Figure 1). As regards regional MBFs during dipyridamole stimulation, they were significantly lower in the mid-distal than in the mid-LV myocardium in controls and in at risk groups with normal and abnormal CTA (2.20 ± .51 vs 2.29 ± .51, 1.56 ± .42 vs 1.91 ± .46, and 1.18 ± .34 vs 1.51 ± .40 mL/g/min, respectively, $P < .0001$), resulting in a longitudinal MBF difference that was the highest in at risk group with normal CTA, intermediate in at risk group with abnormal CTA, and the lowest in controls (Table 2) (Figure 1). In addition, the longitudinal MBF difference during pharmacologic vasodilation was also significantly higher in at risk group with normal CTA than with abnormal CTA ($P < .0002$). Similarly, the change in longitudinal MBF difference from rest to hyperemia defined as Δ longitudinal MBF difference (longitudinal MBF difference during hyperemia minus longitudinal MBF difference at rest) was significantly higher in at risk groups with normal and abnormal CTA as compared to controls (Table 2; Figure 2). Further, the Δ longitudinal MBF difference was significantly higher in at risk with normal CTA than in those with abnormal CTA. The group comparison of the Δ longitudinal MBF differences in controls was significant compared to the at risk groups ($P < .0001$ by ANOVA).

When the longitudinal MBF difference was divided into subgroups by the three major coronary vascular territories (LAD, LCx, and RCA), no significant difference in longitudinal MBF difference between these vascular territories for each group at rest and during pharmacologically induced hyperemic flows was denoted by ANOVA (Table 3). Further, to verify whether

Figure 1. Longitudinal MBF difference in the three study groups at rest and during pharmacologically induced hyperemia.

Figure 2. Δ longitudinal MBF difference (longitudinal MBF difference during hyperemia minus longitudinal MBF difference at baseline) in the three study groups.
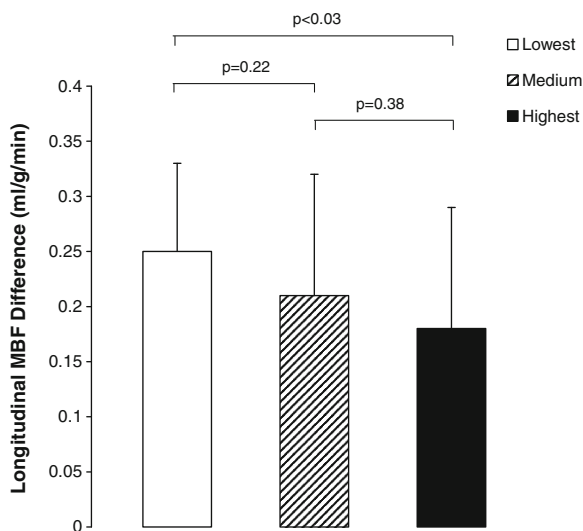
Table 3. Regional longitudinal MBF differences

Longitudinal MBF difference	Controls			At risk with normal CTA			At risk with abnormal CTA		
	LAD	LCx	RCA	LAD	LCx	RCA	LAD	LCx	RCA
At rest	.07 ± .06	.04 ± .03	.07 ± .04	.12 ± .12	.11 ± .13	.08 ± .10	.10 ± .08	.07 ± .09	.09 ± .09
During DP	.10 ± .08	.11 ± .08	.09 ± .10	.33 ± .16	.30 ± .21	.38 ± .20	.23 ± .10	.20 ± .10	.22 ± .14

MBF, Myocardial blood flow (mL/g/min); *DP*, dipyridamole.
P = NS by ANOVA within groups.

CAC exerts downstream effects on coronary flows in at risk group with abnormal CTA and CAC, the effects of regional CAC on corresponding longitudinal MBF difference were evaluated by tertile analysis. The longitudinal MBF difference at rest did not differ significantly among the lowest, the medium, and the highest tertile of log-CCS (.07 ± .08 vs .11 ± .09 vs .08 ± .12 mL/g/min). Conversely, during pharmacologically induced hyperemic flows, the longitudinal MBF difference was non-significantly higher in the lowest as compared to the medium tertile of log-CCS (.25 ± .08 vs .21 ± .11 mL/g/min), whereas it was significantly higher than in the highest tertile of log-CCS (.25 ± .08 vs .18 ± .11 mL/g/min) (Figure 3). Although the longitudinal MBF difference during hyperemic flows was higher in the medium than in the highest tertile of log-CCS, it did not reach statistical significance (.21 ± .11

Figure 3. Comparison of longitudinal MBF difference during pharmacologic vasodilation among cardiovascular risk individuals with abnormal CTA with the lowest (<69.3 HU), the medium (69.3-361.5 HU), and the highest tertile (>361.5 HU) of log-CCS.

vs .18 ± .11 mL/g/min) (Figure 3). Thus, increases in regional log CCS were accompanied by a significant and progressive decrease in regional longitudinal MBF difference during pharmacologic vasodilation, while this was not observed during rest. The regional log-CCS, however, did not correlate with the corresponding regional longitudinal MBF difference during hyperemic flow stimulation, at rest, and with the Δ longitudinal MBF difference, respectively (r = .12, SEE = .99; P = .36, r = .15, SEE = .98; P = .25, and r = .22, SEE = .97; P = .10). Finally, we also evaluated a possible association between the mean proximal artery diameter and longitudinal MBF difference. Also here, no association between the mean proximal artery diameter and the corresponding regional longitudinal MBF difference during hyperemic flow stimulation and at rest, respectively, in controls (r = .28, SEE = .04; P = .17 and r = .15, SEE = .21; P = .48), in cardiovascular risk with normal CTA (r = .16, SEE = .18; P = .94 and r = .08, SEE = .10; P = 0.70), and in cardiovascular risk with abnormal CTA (r = .13, SEE = .09; P = .53 and r = .18, SEE = .11; P = .43) was observed.

Rest to Stress Change in Longitudinal MBF Difference and Hyperemic Flows

As denoted in Figure 4A, the rest to stress Δ longitudinal MBF differences in at risk group with normal and abnormal CTA correlated significantly with the mid-LV MBF during pharmacologically induced hyperemia (r = .62, SEE = .10; P < .0001), implicating the increase in coronary blood flow as an determinant of the Δ longitudinal MBF differences. This finding was further emphasized when patients in at risk groups with normal and abnormal CTA were analyzed separately (Figure 4B, C). Also here, the Δ longitudinal MBF difference in both at risk groups with normal and abnormal CTA was significantly associated with the mid-LV MBF during pharmacologic vasodilation, respectively (r = .52, SEE = .12; P < .007 and r =
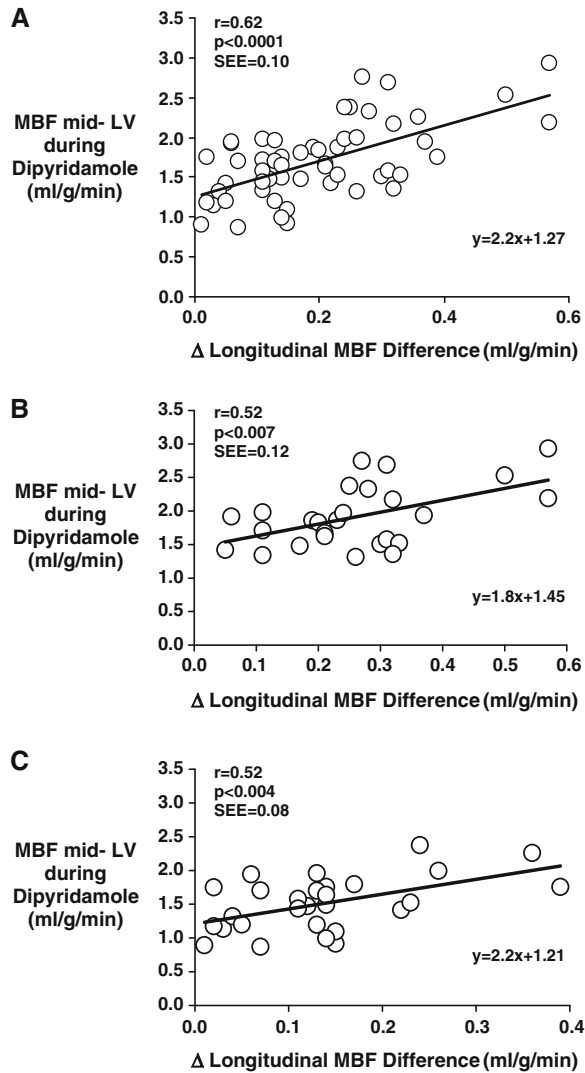
Figure 4. Correlation between MBF mid-LV during dipyridamole and Δ longitudinal MBF difference in all cardiovascular risk individuals (**A**); and in those with normal CTA (**B**); and with abnormal CTA (**C**).

.52, SEE = .08; $P < .004$), not observed in controls ($r = .07$, SEE = .05; $P = .73$).

Determinants of Δ Longitudinal MBF Differences

In the study group as a whole, on univariate analysis, BMI and hyperemic MBF in the mid-LV were significantly associated with Δ longitudinal MBF difference (Table 4). In addition, we performed a multivariate analysis to identify predictors of the Δ longitudinal MBF difference, by which structural alterations of the epicardial wall, as denoted by log-CCS, the hyperemic MBF in the mid-LV, BMI, and smoking were

identified as independent predictors of Δ longitudinal MBF difference. If only at risk groups with normal and abnormal CTA were analyzed, then on univariate analysis log-CCS, hyperemic MBF in the mid-LV and age were significantly associated with Δ longitudinal MBF difference (Table 4). In addition, on multivariate analysis, hyperemic MBF in the mid-LV and triglyceride levels proved to be independent predictors of Δ longitudinal MBF difference.

DISCUSSION

The observations of this study provide first direct evidence that epicardial structural disease and microvascular function are important determinants of an abnormal longitudinal MBF difference in cardiovascular risk individuals, which is assumed to reflect an impairment of a flow-mediated coronary vasodilation. Such findings may agree with the Hagen–Poiseuille law, which denotes the resistance to flow in a tube interacting with serial branches along its length.[27] According to this, the intracoronary resistance depends on the coronary flow velocity and inversely on the fourth power of the vessel diameter, while interacting with branches along its length, that causes flow shunting from the parent artery and the longitudinal perfusion or MBF gradient. As it was observed, the extent of the longitudinal MBF difference was related to the severity of CAC, which has been shown to reflect overall CAD burden,[26] and also to the increase in hyperemic MBF or microvascular function. In cardiovascular risk individuals with CAC, increases in CAC were paralleled by a continuous decrease in the longitudinal MBF difference during pharmacologic vasodilation. An explanation is that with progressive proximal diffuse or segmental narrowing of the proximal parent artery more than distally, proximal resistance at maximal flow may become higher than distal artery resistance such that the gradual longitudinal MBF gradient is reduced or eliminated, again depending on the severity of proximal or distal artery disease and extent of branch disease.[7,9,10] Alternatively, more structural proximal disease may impair downstream distal artery endothelial-mediated vasodilation thereby also reducing the longitudinal MBF gradient. Of further interest, the observed longitudinal MBF difference during hyperemic flows in cardiovascular risk individuals without evidence of epicardial structural disease was more pronounced than in those with structural CAD. In more advanced stages of CAD, as denoted in this study by the presence and severity of calcified and non-calcified coronary plaque burdens, coronary arteriolar function may have already been more severely altered than in those without normal CTA. Advanced stages of microvascular disease in this

Table 4. Univariate and multivariate analysis

| | Δ Longitudinal MBF difference | | | |
| | Univariate analysis | | Multivariate analysis | |
	PCC	P-value	Coefficient β (95% CI)	P-value
Entire study group				
Log-CCS	.08	.469	−.394 (−.084 to .003)	*.034*
MBF mid-LV (mL/g/min)	.09	.450	.382 (.012-.169)	*.025*
Age (years)	.15	.194	.315 (.000-.005)	.115
Sex (male/female)	.13	.249	−.144 (−.112 to .032)	.273
BMI (kg/m^2)	.30	*.007*	.271 (.000-.009)	*.055*
SBP (mmHg)	.07	.515	−.051 (−.003 to .002)	.705
Total cholesterol (mg/dL)	.10	.391	.064 (−.002 to .002)	.845
LDL cholesterol (mg/dL)	.13	.261	.182 (−.002 to .003)	.544
HDL cholesterol (mg/dL)	.09	.445	−.262 (−.005 to .001)	.156
Triglycerides (mg/dL)	.09	.438	−.186 (−.001 to .000)	.174
Glucose (mg/dL)	.17	.145	.181 (.000-.003)	.177
CRP (mg/dL)	.01	.970	.038 (−.003 to .004)	.767
Smoking (pack/years)	.05	.656	.325 (.001-.009)	.028
Cardiovascular risk groups				
Log-CCS	.46	*.0001*	−.271 (−.067 to .014)	.187
MBF mid-LV (mL/g/min)	.62	*.0001*	.529 (.050-.242)	*.004*
Age (years)	.42	*.001*	−.192 (−.005 to .002)	.312
Sex (male/female)	.13	.346	−.045 (−.087 to .062)	.739
BMI (kg/m^2)	.16	.242	−.032 (−.005 to .004)	.839
SBP (mmHg)	.08	.548	−.045 (−.002 to .002)	.752
Total cholesterol (mg/dL)	.11	.412	.015 (−.002 to .002)	.959
LDL cholesterol (mg/dL)	.08	.563	.372 (.000-.004)	.183
HDL cholesterol (mg/dL)	.18	.206	−.070 (−.005 to .003)	.693
Triglycerides (mg/dL)	.20	.145	−.359 (−.002 to .000)	*.021*
Glucose (mg/dL)	.05	.714	.144 (.000-.003)	.292
CRP (mg/dL)	.23	.137	−.025 (−.003 to .003)	.853
Smoking (pack/years)	.21	.132	.211 (−.001 to .006)	.173

PCC, Pearson correlation coefficient; *CCS*, coronary artery calcium score; *MBF*, myocardial blood flow; *BMI*, body mass index; *SBP*, systolic blood pressure; *LDL cholesterol*, low-density lipoprotein cholesterol; *HDL cholesterol*, high-density lipoprotein cholesterol; *CRP*, C-reactive protein.
P-values by ANOVA with significance level ≤0.05.

study population, associated with diminished hyperemic flows, may in fact have offset the magnitude of the longitudinal MBF gradient during pharmacologic vasodilation, resulting in a less marked flow gradient than one might have expected. This may also explain, at least in part, that although increases in CAC were accompanied by a continuous decrease in the longitudinal MBF difference during pharmacologic vasodilation, individual measurements of CAC did not correlate with the longitudinal MBF difference. It is equally possible that the cardiovascular risk group with CAC was not large enough or, conversely, that the range of longitudinal MBF difference during hyperemic flows was not wide enough to result in a statistically significant association.

However, as the intracoronary resistance relates to the velocity of the blood flow, apart from the inverse relation to the vessel diameter according to the Hagen–Poiseuille law, higher increases in hyperemic MBFs in cardiovascular risk individuals with normal CTA, therefore, resulted in relatively higher and abnormal elevations in intracoronary resistance due to an impairment of a flow-mediated coronary vasodilation than in those with abnormal CTA and lower hyperemic flows. This is in line with the observed close correlation between the hyperemic longitudinal MBF difference and the MBF increase in the mid-LV during pharmacologic vasodilation in cardiovascular risk individuals, identifying the magnitude of hyperemic MBF increase as an

important determinant of the abnormal longitudinal MBF difference. Interestingly, a more recent investigation[28] of stress and rest myocardial perfusion imaging with [82]rubidium PET in patients with subclinical CAD described a regional decrease in resting myocardial perfusion, while it was not observed during dipyridamole-stimulated hyperemic flows. This mild longitudinal decrease in resting myocardial perfusion was ascribed to direct downstream effects of diffuse CAD, which appeared to be overcome during hyperemic flow stimulation. A previous invasive coronary angiographic investigation by Schachinger and Zeiher[29] may support this consideration as increasing atherosclerotic wall thickening, determined with intravascular ultrasound, was associated with a decrease in baseline coronary vasomotor tone. Similar observations were reported by Tousoulis et al[30] in that a flow-mediated epicardial vasodilation during coronary flow-increases may not be diminished only during vasomotor stress but also at resting state in patients with structurally diseased coronary arteries and reductions in the diameter of the epicardial artery. Advanced regional structural and/or functional alterations of the coronary circulation, therefore, may possible lead to a relative and mild fall of regional resting flow.[28] These observations may also accord with current findings where MBF quantification demonstrated a mild longitudinal flow difference also at resting condition. Yet, it has to be taken into account for that partial volume effects during the data acquisition in the apical portion of the LV are likely to have contributed to lower apical MBFs and, thereby, to the magnitude of the longitudinal MBF difference. While the reason for these in part contrasting observations[7,9,13,28,31] remains uncertain, it may be related to differences in patients' characteristics and/or differences in the extent of CAD-related structural and functional disease of the epicardial vascular wall.

LIMITATIONS

There are important limitations worthy to be considered in interpreting our data. First, in the cardiovascular risk group with diffuse and most commonly moderate to severe CAC, the blooming artifacts of calcified plaques on CTA did not allow a proper analysis in a substantial number of coronary artery segments. Thus, in this cardiovascular risk group, we cannot exclude that more epicardial lesions with >50% diameter stenosis were indeed present without being identified on CTA due to CAC-induced blooming artifacts, which may have affected coronary flows. On the other hand, normal stress and rest myocardial perfusion on ^{13}N-ammonia PET/CT images, as inclusion criteria in the study population, widely argued against the presence of advanced and flow-limiting of epicardial lesions. Further, left-ventricular ejection fraction was normal at peak stress and rest on gated PET, widely ruling out the presence of hemodynamically significant epicardial lesions of the left main stem or three vessels disease leading to diffuse ischemia. Second, as we did not perform intravascular coronary ultrasound in cardiovascular risk individuals with normal CTA, early and subclinical CAD-related structural alterations of the artery may have been present as well, apart from coronary circulatory dysfunction, and have also contributed to an impairment of flow-mediated epicardial vasodilation with the manifestation of observed hyperemic longitudinal MBF difference. Third, MBFs in the mid and mid-distal left-ventricular segments were measured and, thus, the longitudinal MBF difference was determined over a relatively short longitudinal distance in order to avoid confounding count variability in the basal segments and partial volume effects in the apical segment on MBF measurements.[7] This in fact may have led to an underestimation of the longitudinal MBF difference during hyperemic flows when compared to a different analysis approach as described by Gould et al.[7]

CONCLUSIONS

In cardiovascular risk individuals with normal stress–rest perfusion ^{13}N-ammonia PET/CT perfusion images, epicardial structural disease and microvascular function are important determinants of an abnormal longitudinal MBF difference, reflecting effects of early coronary atherosclerosis without segmental flow-limiting stenosis, but needing further clinical investigation.

Acknowledgments

References

1. Camici PG, Rimoldi OE. The clinical value of myocardial blood flow measurement. J Nucl Med 2009;50:1076-87.
2. Schindler TH, Zhang XL, Vincenti G, Mhiri L, Lerch R, Schelbert HR. Role of PET in the evaluation and understanding of coronary physiology. J Nucl Cardiol 2007;14:589-603.

3. Schindler TH, Nitzsche EU, Olschewski M, Brink I, Mix M, Prior J, et al. PET-measured responses of MBF to cold pressor testing correlate with indices of coronary vasomotion on quantitative coronary angiography. J Nucl Med 2004;45:419-28.

4. Schindler TH, Schelbert HR, Quercioli A, Dilsizian V. Cardiac PET imaging for the detection and monitoring of coronary artery disease and microvascular health. JACC Cardiovasc Imaging 2010;3:623-40.

5. Kaufmann PA, Camici PG. Myocardial blood flow measurement by PET: Technical aspects and clinical applications. J Nucl Med 2005;46:75-88.

6. Schelbert HR. Anatomy and physiology of coronary blood flow. J Nucl Cardiol 2010 [Epub ahead of print].

7. Gould KL, Nakagawa Y, Nakagawa K, Sdringola S, Hess MJ, Haynie M, et al. Frequency and clinical implications of fluid dynamically significant diffuse coronary artery disease manifest as graded, longitudinal, base-to-apex myocardial perfusion abnormalities by noninvasive positron emission tomography. Circulation 2000;101:1931-9.

8. Sdringola S, Patel D, Gould KL. High prevalence of myocardial perfusion abnormalities on positron emission tomography in asymptomatic persons with a parent or sibling with coronary artery disease. Circulation. 2001;103:496-501.

9. Hernandez-Pampaloni M, Keng FY, Kudo T, Sayre JS, Schelbert HR. Abnormal longitudinal, base-to-apex myocardial perfusion gradient by quantitative blood flow measurements in patients with coronary risk factors. Circulation 2001;104:527-32.

10. Schindler TH, Facta AD, Prior JO, Campisi R, Inubushi M, Kreissl MC, et al. PET-measured heterogeneity in longitudinal myocardial blood flow in response to sympathetic and pharmacologic stress as a non-invasive probe of epicardial vasomotor dysfunction. Eur J Nucl Med Mol Imaging 2006;33:1140-9.

11. Schindler TH, Zhang XL, Vincenti G, Mhiri L, Nkoulou R, Just H, et al. Diagnostic value of PET-measured heterogeneity in myocardial blood flows during cold pressor testing for the identification of coronary vasomotor dysfunction. J Nucl Cardiol 2007;14:688-97.

12. De Bruyne B, Hersbach F, Pijls NH, Bartunek J, Bech JW, Heyndrickx GR, et al. Abnormal epicardial coronary resistance in patients with diffuse atherosclerosis but ''Normal'' coronary angiography. Circulation 2001;104:2401-6.

13. Schindler TH, Facta AD, Prior JO, Cadenas J, Zhang XL, Li Y, et al. Structural alterations of the coronary arterial wall are associated with myocardial flow heterogeneity in type 2 diabetes mellitus. Eur J Nucl Med Mol Imaging 2009;36:219-29.

14. Gould KL, Pan T, Loghin C, Johnson NP, Guha A, Sdringola S. Frequent diagnostic errors in cardiac PET/CT due to misregistration of CT attenuation and emission PET images: A definitive analysis of causes, consequences, and corrections. J Nucl Med 2007;48:1112-21.

15. Hachamovitch R, Berman DS, Shaw LJ, Kiat H, Cohen I, Cabico JA, et al. Incremental prognostic value of myocardial perfusion single photon emission computed tomography for the prediction of cardiac death: Differential stratification for risk of cardiac death and myocardial infarction. Circulation 1998;97:535-43.

16. Dilsizian V, Bacharach SL, Beanlands RS, Bergmann SR, Delbeke D, Gropler RJ, et al. PET myocardial perfusion and metabolism clinical imaging. J Nucl Cardiol. 2009;16:651.

17. DeGrado TR, Hanson MW, Turkington TG, Delong DM, Brezinski DA, Vallee JP, et al. Estimation of myocardial blood flow for longitudinal studies with 13N-labeled ammonia and positron emission tomography. J Nucl Cardiol 1996;3:494-507.

18. Cerqueira MD, Weissman NJ, Dilsizian V, Jacobs AK, Kaul S, Laskey WK, et al. Standardized myocardial segmentation and nomenclature for tomographic imaging of the heart: A statement for healthcare professionals from the Cardiac Imaging Committee of the Council on Clinical Cardiology of the American Heart Association. Circulation 2002;105:539-42.

19. Koepfli P, Wyss CA, Namdar M, Klainguti M, von Schulthess GK, Luscher TF, et al. Beta-adrenergic blockade and myocardial perfusion in coronary artery disease: Differential effects in stenotic versus remote myocardial segments. J Nucl Med 2004;45:1626-31.

20. Gambhir SS, Schwaiger M, Huang SC, Krivokapich J, Schelbert HR, Nienaber CA, et al. Simple noninvasive quantification method for measuring myocardial glucose utilization in humans employing positron emission tomography and fluorine-18 deoxyglucose. J Nucl Med 1989;30:359-66.

21. Muzik O, Beanlands RS, Hutchins GD, Mangner TJ, Nguyen N, Schwaiger M. Validation of nitrogen-13-ammonia tracer kinetic model for quantification of myocardial blood flow using PET. J Nucl Med 1993;34:83-91.

22. Hutchins GD, Schwaiger M, Rosenspire KC, Krivokapich J, Schelbert H, Kuhl DE. Noninvasive quantification of regional blood flow in the human heart using N-13 ammonia and dynamic positron emission tomographic imaging. J Am Coll Cardiol 1990;15:1032-42.

23. Husmann L, Valenta I, Gaemperli O, Adda O, Treyer V, Wyss CA, et al. Feasibility of low-dose coronary CT angiography: first experience with prospective ECG-gating. Eur Heart J 2008;29:191-7.

24. Austen WG, Edwards JE, Frye RL, Gensini GG, Gott VL, Griffith LS, et al. A reporting system on patients evaluated for coronary artery disease. Report of the Ad Hoc Committee for Grading of Coronary Artery Disease, Council on Cardiovascular Surgery, American Heart Association. Circulation 1975;51:5-40.

25. van Werkhoven JM, Schuijf JD, Gaemperli O, Jukema JW, Boersma E, Wijns W, et al. Prognostic value of multislice computed tomography and gated single-photon emission computed tomography in patients with suspected coronary artery disease. J Am Coll Cardiol 2009;53:623-32.

26. Rumberger JA, Simons DB, Fitzpatrick LA, Sheedy PF, Schwartz RS. Coronary artery calcium area by electron-beam computed tomography and coronary atherosclerotic plaque area. A histopathologic correlative study. Circulation 1995;92:2157-62.

27. Gould KL, Lipscomb K, Calvert C. Compensatory changes of the distal coronary vascular bed during progressive coronary constriction. Circulation 1975;51:1085-94.

28. Johnson NP, Gould KL. Clinical evaluation of a new concept: resting myocardial perfusion heterogeneity quantified by markovian analysis of PET identifies coronary microvascular dysfunction and early atherosclerosis in 1, 034 subjects. J Nucl Med 2005;46:1427-37.

29. Schachinger V, Zeiher AM. Quantitative assessment of coronary vasoreactivity in humans in vivo. Importance of baseline vasomotor tone in atherosclerosis. Circulation 1995;92:2087-94.

30. Tousoulis D, Davies GJ, Tentolouris C, Crake T, Lefroy DC, Toutouzas P. Effects of inhibition of nitric oxide synthesis in patients with coronary artery disease and stable angina. Eur Heart J 1997;18:608-13.

31. Sdringola S, Loghin C, Boccalandro F, Gould KL. Mechanisms of progression and regression of coronary artery disease by PET related to treatment intensity and clinical events at long-term follow-up. J Nucl Med 2006;47:59-67.